PHOTONICS Research

All-dielectric photonic crystal with unconventional higher-order topology

Shiqiao Wu,[1,2] Bin Jiang,[1,2] Yang Liu,[1,2] and Jian-Hua Jiang[1,2,3,*]

[1]School of Physical Science and Technology, Soochow University, Suzhou 215006, China
[2]Collaborative Innovation Center of Suzhou Nano Science and Technology, Suzhou 215006, China
[3]Key Lab of Advanced Optical Manufacturing Technologies of Jiangsu Province and Key Lab of Modern Optical Technologies of Ministry of Education of China, Soochow University, Suzhou 215006, China
*Corresponding author: jianhuajiang@suda.edu.cn

Received 30 December 2020; revised 18 February 2021; accepted 18 February 2021; posted 22 February 2021 (Doc. ID 418689); published 15 April 2021

Photonic crystals (PhCs) have been demonstrated as a versatile platform for the study of topological phenomena. The recent discovery of higher-order topological insulators introduces new aspects of topological PhCs that are yet to be explored. Here, we propose an all-dielectric PhC with an unconventional higher-order band topology. Besides the conventional spectral features of gapped edge states and in-gap corner states, topological band theory predicts that the corner boundary of the higher-order topological insulator hosts a 2/3 fractional charge. We demonstrate that in the PhC such a fractional charge can be verified from the local density-of-states of photons, through the concept of local spectral charge as an analog of the local electric charge due to the band filling anomaly in electronic systems. Furthermore, we show that by introducing a disclination in the proposed PhC, localized states and a 2/3 fractional spectral charge emerge around the disclination core. The emergence of the fractional spectral charges and topological boundary modes here, however, is distinct from the known cases; particularly by the 2/3 fractional spectral charges and the unique topological indices. The predicted effects can be readily observed in the state-of-the-art experiments and may lead to potential applications in integrated and quantum photonics.

https://doi.org/10.1364/PRJ.418689

1. INTRODUCTION

Topological insulators, which host gapped bulk states and robust gapless edge states [1–4], brought new concepts and ideas in photonics in the past decade. Topologically protected photonic edge states can serve as robust waveguides, which have been demonstrated to be useful in integrated photonics [5–9], information transport [10–17], quantum photonics [18,19], lasing [20–28], and exciton-polariton devices [29–31]. The ability to visualize the wavefunctions of the bulk and edge photonic states as well as the controllability of photonic systems makes them a highly desirable platform for the study of topological phenomena.

Recently, it was predicted [30–39] and observed [40–68] that topological boundary states can emerge not only on the boundaries with $n-1$ dimensions, but also on the boundaries with $n-2$ and lower dimensions of n-dimensional (nD) topological insulators. Such exotic topological insulators are termed as higher-order topological insulators (HOTIs) [30–39]. For instance, a two-dimensional (2D) HOTI hosts 1D edge states at the edge boundaries as well as 0D corner states at the corner boundaries [30–39]. The underlying mechanism is that, due to the intricate role of the crystalline symmetry, the 1D edge states become gapped and hence can be regarded as emergent 1D insulators. At the corner boundaries between the edge boundaries, the 0D corner states emerge in the common band gap of the edge and bulk states due to edge or bulk band topology [30–68]. Such topologically protected multidimensional boundary states beyond the bulk-edge correspondence introduce new degrees of freedom in the design of photonic states for wave-guiding, trapping, and manipulation, which may lead to potential applications in integrated photonics, quantum photonics, and high-performance lasing [57–71]. However, such a discipline is still at its infant stage and yet to be fully developed. In particular, hexagonal photonic crystals (PhCs) with the six-fold rotation (C_6) crystalline symmetry are well-known for hosting topological edge states [11,12,15,18,72–75] and can also support higher-order band topology [43,65]. Such PhCs, when made of all dielectric materials, host promising applications in advanced photonic and quantum technology [18,74,75].

In this work, we propose an all-dielectric hexagonal PhC that exhibits a topological band gap as the photonic analog of an unprecedented topological crystalline insulator.

The unique band topology, as protected by the C_6 crystalline symmetry, is manifested first by the coexisting gapped edge states and in-gap corner states, indicating a photonic HOTI. From topological band theory, the photonic HOTI hosts a fractional corner charge of $Q_c = 2/3$. We demonstrate, using the first-principle simulations, that such a fractional charge can be verified through the concept of local spectral charge as an analog of the local electric charge due to a band filling anomaly in electronic systems. Physically, the spectral charge measures how many photonic modes exist in a local area in a given frequency range. Exploiting such a concept, we further show that disclinations, topological defects that disrupt the crystalline rotation symmetry, can induce a fractional spectral charge $Q_{\text{dis}} = 2/3$ and trap localized photonic states around the disclination core. We emphasize that the all-dielectric PhC proposed here hosts what we believe, to the best of our knowledge, is an unprecedented higher-order band topology that is particularly reflected by the unique topological indices and the fractional spectral charge of $2/3$. In comparison, previous studies focused on cases with 1/2 fractional spectral charges [76]. First-principle calculations give consistent results with the bulk-disclination correspondence picture predicted by the topological band theory. The unique topological phenomena found in this work can be readily observed in the state-of-the-art photonic experiments and may offer potential applications in topological quantum photonics and topological lasing.

This paper has seven sections. Section 2 focuses on the design of the PhC and its bulk topological indices. Section 3 studies the topological edge and corner states as well as the fractional corner charge. Section 4 explores the manifestation of the bulk-disclination correspondence in the PhC. Section 5 demonstrates the disclination in the trivial PhC. Section 6 shows the robustness of the disclination states. Section 7 gives the conclusions and outlooks.

2. PHOTONIC CRYSTAL AND BULK TOPOLOGICAL INDICES

We propose a hexagonal PhC with six dielectric cylindrical rods in each unit cell [see Fig. 1(a)] to realize the above topological effects. We focus on the lowest few photonic bands of transverse-magnetic harmonic modes. Despite that our PhC looks a bit similar to the PhC proposed by Wu and Hu (denoted hereafter as Wu–Hu's PhC) [11], their topological indices and properties are distinct. First, there are only two bands below the topological gap in our PhC; Wu–Hu's PhC, however, has three bands below the topological gap. Moreover, the band symmetry representations and the topological indices are distinct for the two PhCs, as elaborated below.

The photonic band gaps discussed here are analogs of topological crystalline insulators protected by the C_6 crystalline symmetry. In this context, the topological indices of the band gap can be deduced from the symmetry indicators of the bands below the gap. Using the theory in Ref. [39], the topological indices are given by

$$\chi^{(6)} = (\chi_M, \chi_K). \tag{1}$$

Here, the symmetry indicators are $\chi_M = \#M_1^{(2)} - \#\Gamma_1^{(2)}$ and $\chi_K = \#K_1^{(3)} - \#\Gamma_1^{(3)}$, respectively. The symbol $\#\Pi_l^{(n)}$ denotes the number of bands with the C_n rotation eigenvalue $e^{i2\pi(l-1)/n}$ $(l = 1, \ldots, n)$ below the band gap at a high-symmetry point $\Pi = \Gamma, M, K$. The symbol χ_M (χ_K) thus stands for the change of the symmetry representations between the M (K) and the Γ points. For instance, χ_M represents the parity inversion between the Γ and M points, as generalized parity-inversion [1] (or generalized Fu–Kane [2]) indices. According to the symmetry eigenvalues at the high symmetry points [as illustrated in Figs. 1(b) and 1(c)], we find that our PhC has $\chi^{(6)} = (0, -2)$, whereas Wu–Hu's PhC (also studied recently in Ref. [76]) has $\chi^{(6)} = (-2, 0)$. Moreover, Wu–Hu's PhC has a nontrivial second Stiefel–Whitney number $\nu = 1$ [i.e., $4m + 2$ (where m is an integer) odd-parity Bloch states at all time-reversal invariant momenta (the Γ point and the three M points)], whereas our PhC here has a trivial second Stiefel–Whitney number $\nu = 0$ (i.e., $4m$ odd-parity Bloch states at all time-reversal invariant momenta), according to Ref. [77].

Geometrically, the key difference between our PhC and Wu–Hu's PhC is that in our PhC, the dielectric rods are aligned along the line from the corners to the center of the unit cell [see the brown dashed line in the inset of Fig. 1(a)]. In comparison, in Wu–Hu's PhC the dielectric rods are aligned from the edge centers to the center of the unit cell, as shown by the green dotted line in the inset of Fig. 1(a).

The evolution of the lowest six photonic bands with the geometry parameter d (i.e., the distance between the rod center and the unit cell center), is presented in Figs. 1(d) and 1(e). From Fig. 1(e), one can see that only the band gap between the second and the third bands is topological, whereas the other band gaps are all trivial (i.e., these band gaps have trivial indices $\chi_M = \chi_K = 0$). We find that the topological band gap is finite only when $d > 0.418a$.

Although the results in this paper do not depend on the lattice constant (since the Maxwell's equations are scale-invariant), most of the calculations here focus on the situation with $a = 25$ mm and $d = 0.47a$ (unless specified as other values), while the relative dielectric constant and the diameter of the rods are $\varepsilon_d = 24$ and $D = 4$ mm, respectively. At microwave frequencies, such dielectric rods can be realized using zirconia ceramics. For these parameters, we find a bulk band gap ranging from 4.0 GHz to 5.15 GHz, yielding a large photonic band gap. Moreover, we find that for the same geometry parameters specified above, when the relative permittivity ε_d varies, the topological photonic band gap survives for permittivity larger than 9 [see Figs. 1(f) and 1(g)]. In the near-infrared regime, silicon has a permittivity as large as 13, which is sufficiently large to induce the topological photonic band gap proposed in this work.

3. TOPOLOGICAL EDGE AND CORNER STATES AND THE FRACTIONAL CORNER CHARGE

As a consequence of the nontrivial topological band gap, topological edge and corner states emerge in finite structures. To demonstrate this, we first consider a structure that is finite along the y direction, but periodic along the x direction [see Figs. 2(a) and 2(b)]. Hard-wall boundary conditions are imposed at the two terminating edges in the y direction that are simulated using the perfect electrical conductor (PEC)

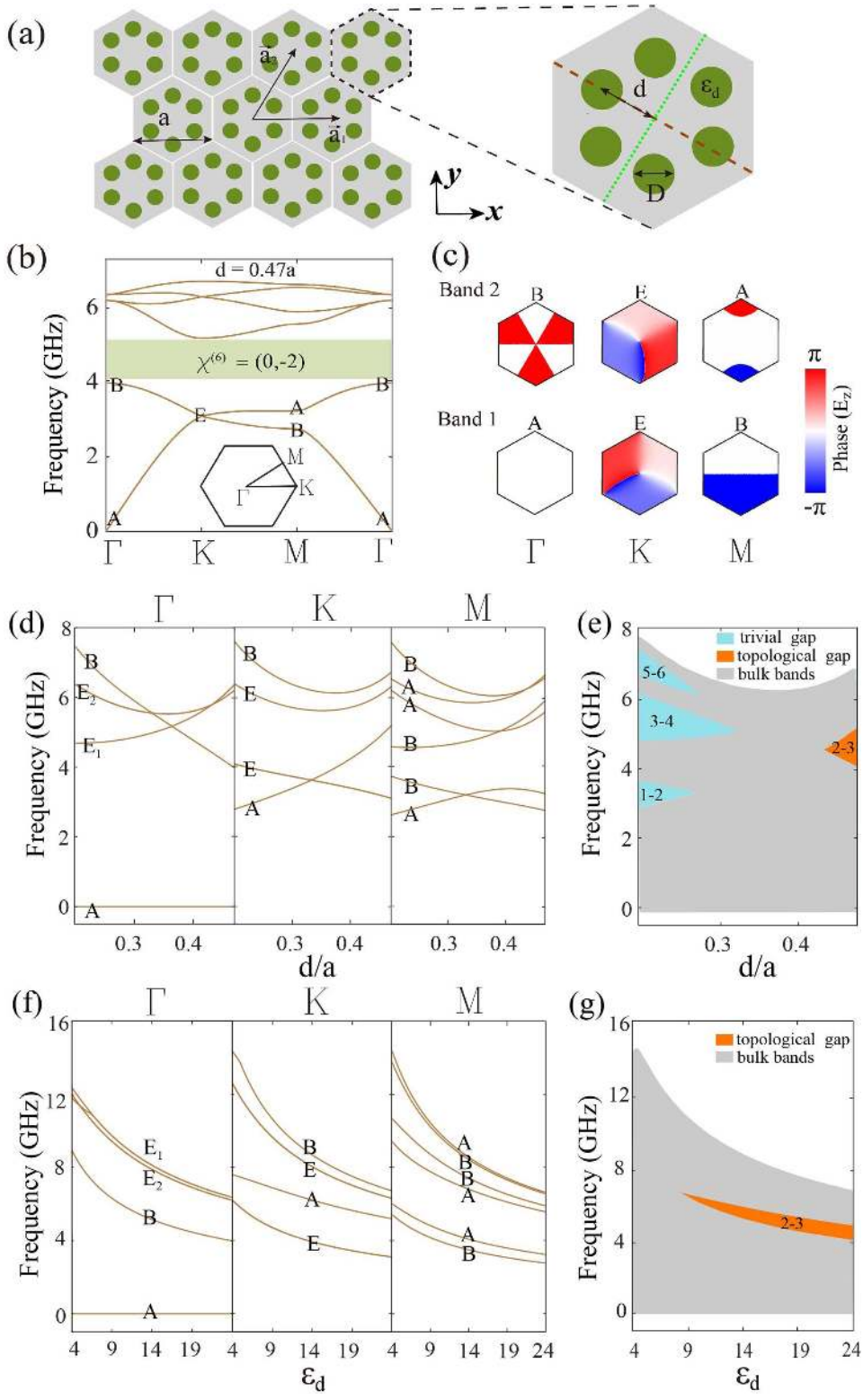

Fig. 1. (a) Schematic illustration of the 2D hexagonal PhC. Inset shows the zoom-in structure of the unit cell. Gray region is air, while the green dots denote the dielectric rods with a diameter $D = 4$ mm and a relative permittivity $\varepsilon_d = 24$. The lattice vectors of the hexagonal lattice, $\vec{a}_1$ and $\vec{a}_2$, are depicted. The lattice constant is $a = 25$ mm, while the distance between the center of a rod and the unit cell center, d, is tunable. (b) Photonic band structure for $d = 0.47a$. The photonic band gap (green region) has a nontrivial topological index of $\chi^{(6)} = (0, -2)$. The little group representations (i.e., A, B, and E) are labeled on the band structure. The phase profiles for the electric field E_z of the corresponding Bloch states are shown in (c). (d) Evolutions of the first six bands at the high symmetry points, Γ, M, and K, with the geometry parameter d. (e) Evolutions of the bulk bands (frequency ranges) and the band gaps with the parameter d. (f) Evolutions of the first six bands at the high symmetry points, Γ, M, and K, with the relative permittivity ε_d. (g) Evolutions of the bulk bands (frequency ranges) and the band gaps with the relative permittivity ε_d.

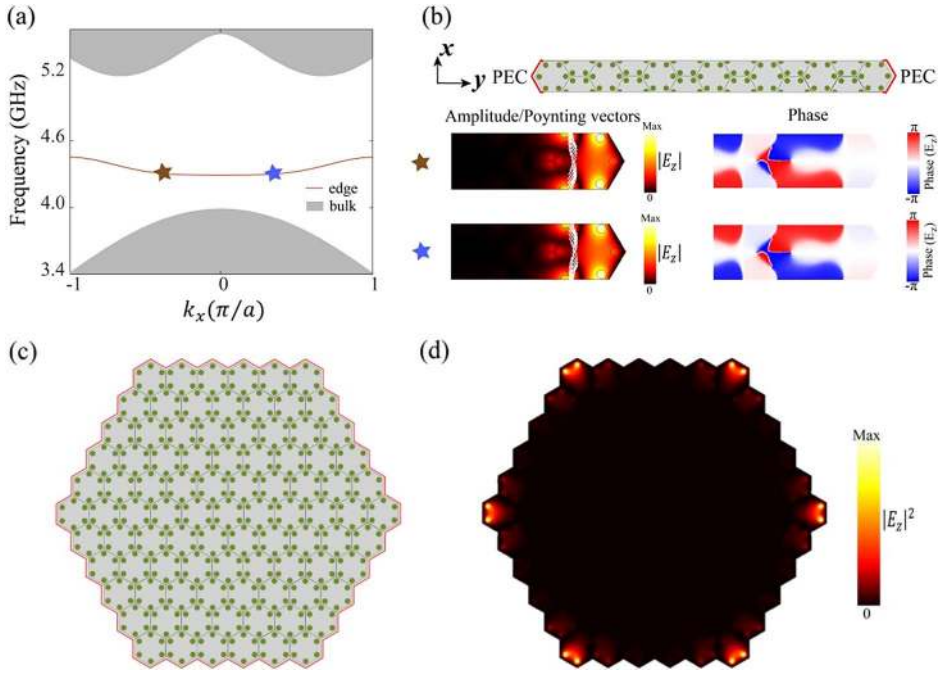

Fig. 2. (a) Photonic dispersions at the bulk, edge, and corners. Both the bulk and edge dispersions are calculated using the structure illustrated in the upper panel of (b). The corner frequency is calculated from the finite structure illustrated in (c). Upper panel of (b): Structure for the study of the edge states, which is finite along the y direction but periodic in the x direction. PEC boundaries are imposed at the left and right ends of the structure. Lower panels of (b): Amplitude and phase profiles of the electric field E_z for the two edge states labeled by the stars in (a). (c) Illustration of the finite structure used to study the corner states. (d) Distribution of the summed electric field intensity for all the corner states. There are six degenerate corner states, as shown in Fig. 3(a). In all calculations, a thin layer of air with a width of $0.08a$ is set between the PEC boundary and the PhC.

boundaries (i.e., metallic boundaries for far-infrared and microwave photons), as shown in Fig. 2(b). A calculation indicates that the edge states are gapped and only one branch of the edge states emerges in the bulk band gap, as shown in Fig. 2(a). The dispersion of the edge states tends to be flat instead of gapless and dispersive. Such edge states are quite different from the known photonic edge states in the literature [5–17,72–75]. Not that similar edge states were found recently in Ref. [69]. The amplitude and phase profiles of the electric field E_z as well as the distributions of the Poynting vectors, which are shown in Fig. 2(b), agree with the time-reversal symmetry for the two edge states with opposite wavevectors.

When the PhC is finite in all directions, as depicted in Fig. 2(c), both the edge and corner states emerge. There are six nearly degenerate corner states emerging in the common band gap of the bulk and the edge states, as shown in Fig. 3(a). Each of them is localized at one of the corner boundary, as indicated by the distribution of the summed electric field intensity $|E_z|^2$ for all the corner states, as shown in Fig. 2(d).

In addition to the edge and corner states, topological band theory predicts that in finite systems, a fractional electric charge appears at the corner boundary due to the filling anomaly of the occupied bulk bands in electronic systems [39]. The fractional part of the corner charge, eQ_c, is connected to the bulk topological indices through [39]

$$Q_c = \left(\frac{1}{4}\chi_M + \frac{1}{6}\chi_K\right) \bmod 1. \tag{2}$$

The equation above states that the fractional corner charge is determined by the bulk band topology. In electronic systems, the fractional corner charge is directly related to the local electric charge. However, photons are neutral particles that lack such a property. Nevertheless, it has been shown that through the concept of "spectral charge," the fractional corner charge can still be measured in bosonic systems [78].

To verify the fractional corner charge in photonic systems, we calculate the spectral charge for each unit cell in the structure illustrated in Fig. 3(c). Specifically, the spectral charge for the p-th unit cell in the structure is defined as

$$Q_p = \int_0^{f_{\text{gap}}} \mathrm{d}f \int_{\substack{p\text{-th}\\ \text{U.C.}}} \mathrm{d}\vec{r}\,\rho(f,\vec{r}), \tag{3}$$

where f_{gap} is a frequency in the common band gap of the bulk and edge states, and $\rho(f,\vec{r})$ is the local density of states (LDOS) of photons (f is the frequency and $\vec{r}$ is the position vector). The integration over the coordinates is performed for the region of the p-th unit cell. The equation above is an analog of the electric charge for the p-th unit cell by band filling up to the Fermi energy in the bulk band gap in electronic systems. For topologically trivial insulators, for each unit cell Q_p is equal to the number of bands below the band gap [39], which is consistent with the picture that each unit cell contributes Q_p modes to form the bulk bands below the trivial band gap. However, for topological crystalline insulators, fractional spectral charges can appear due to band filling anomaly [39]. We remark that the applications of the PEC boundary are

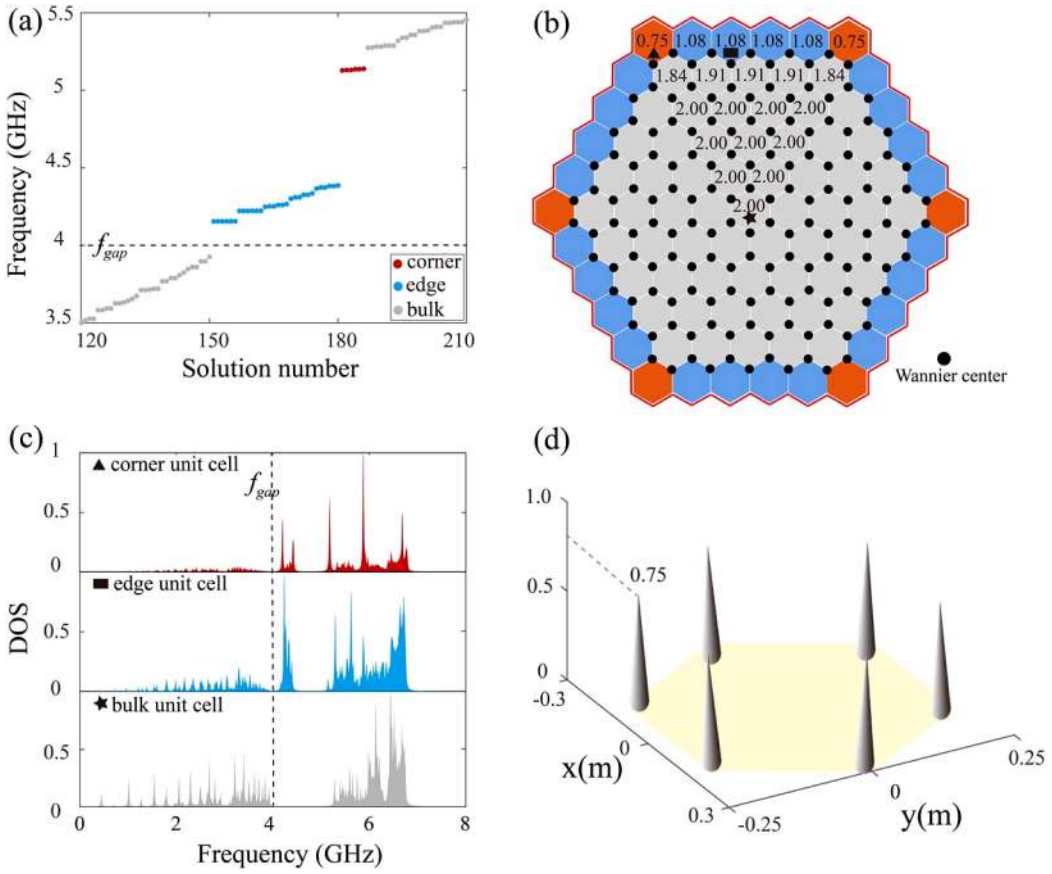

Fig. 3. (a) Photonic spectrum for the finite PhC structure illustrated in Fig. 2(c). Only the eigenstates in and around the bulk band gap are shown. (b) Spectral charges for various unit cells. The gray region denotes the bulk. The blue region denotes the edges, while the red region denotes the corners. (c) Local density-of-states (DOS) for photons in three different types of unit cells labeled by the triangle (corner unit cell), rectangle (edge unit cell), and the star (bulk unit cell). Integrating the photonic LDOS up to the frequency $f_{\text{gap}} = 4$ GHz gives rise to fractional spectral charges at the corner boundaries. (d) Illustration of the distribution of the fractional corner charges in a finite sample. In all calculations, a thin layer of air with the width $0.08a$ is set between the PEC boundary and the PhC.

important here for the evaluation of the fractional mode charge. Particularly, the PEC boundary confines the photons in a finite supercell and makes the system closed and Hermitian; therefore, the boundary preserves the quantization of the fractional charges.

We calculate the photonic LDOS and obtain the spectral charges for all the unit cells. The photonic spectral charge for each unit cell can be obtained by integrating the photonic LDOS $\rho(f,\vec{r})$ up to a frequency in the band gap, f_{gap}, as indicated by Eq. (3). The LDOS is calculated through the photonic eigenstates. If we denote the wavefunction of the i-th photonic eigenstate as ψ_i and the frequency of the eigenstate as f_i, then the LDOS can be written as

$$\rho(f,\vec{r}) = \sum_i \frac{\Gamma}{\pi[\Gamma^2 + (f - f_i)^2]} |\psi_i(\vec{r})|^2. \tag{4}$$

Here, Γ is a parameter used to model the Lorentz broadening of the eigenstates. In our calculation, Γ is set to be sufficiently small to converge the calculation. The normalized photonic wavefunction is given by

$$|\psi_i(\vec{r})|^2 = \varepsilon(\vec{r})|E_{z,i}(\vec{r})|^2, \tag{5}$$

where $\varepsilon(\vec{r})$ is the relative permittivity and $E_{z,i}(\vec{r})$ is the rescaled electric field of the i-th photonic eigenstate that satisfies $\int d\vec{r}\varepsilon(\vec{r})|E_{z,i}(\vec{r})|^2 = 1$. The spectral charge is then given by Eq. (3), where the integration over the coordinates is performed for the region of the p-th unit cell.

Based on the calculation method above, we find that in the bulk region (gray), the spectral charge is nearly 2 for each unit cell in Fig. 3(b). In comparison, in the edge region (blue), the spectral charge is close to 1 for each unit cell, while in the corner region (red), the spectral charge is close to 2/3.

The above spectral charges can be understood through the Wannier centers. In our photonic system, there are only bulk states below the frequency $f_{\text{gap}} = 4$ GHz. These bulk modes are pictorially represented by the Wannier centers away from the edge and corner boundaries. In each bulk unit cell, there are six Wannier centers locating at the corners of the unit cell. Each Wannier center is shared by three neighboring unit cells, thus contributing 1/3 spectral charge to one of these unit cells. Therefore, each bulk unit cell has a spectral charge of 2 (i.e., there are two photonic modes in each bulk unit cell). These two modes interact with the modes in other unit cells and form the two bulk Bloch bands below the band gap.

In comparison, there are three Wannier centers in an edge unit cell. The other three Wannier centers in the edge unit cell are obstructed by the edge boundary and become edge states. For a corner unit cell, there are only two Wannier centers associated with the bulk, while the other four Wannier centers are obstructed by the boundary and become edge and corner states. As a consequence, an edge unit cell has a spectral charge 1, while a corner unit cell has a spectral charge 2/3.

Our first-principle calculations give a spectral charge 1.07 for an edge unit cell that is close to the theoretical value 1. On the other hand, each corner unit cell has a spectral charge 0.75 that is not far away from the theoretical value 2/3. In general, because PhCs are in the continuum limit, the PEC boundaries may slightly affect the specific mode charges. The corner unit cells have three facets with the PEC boundaries and thus are more affected by such effects, compared to the edge unit cells that have two facets with the PEC boundaries. Note that the charge has to be fractionalized to integer times of 1/3 or 1/2, not to other fractional values, according to Eqs. (2) and (6). Therefore, the small deviations of the numerical value of the corner (and disclination) charge from the theoretical value do not cause a problem in identifying the correct fractional corner or disclination charges. The slight deviation of the spectral charges calculated using the first-principle methods from the theoretical spectral charges essentially originates from the fact that photons in PhCs do not strictly follow the tight-binding theory. Nevertheless, the fractional corner charge is still revealed approximately from the first-principle calculations.

4. BULK-DISCLINATION CORRESPONDENCE

We now study the bulk-disclination correspondence in our higher-order topological PhC. The bulk-disclination correspondence predicts that in topological crystalline insulators, the fractional charge bound to a disclination with a Frank angle Ω is determined by the symmetry indicators of the Bloch bands below the band gap [76,78,79], so

$$Q_{\mathrm{dis}} = \frac{\Omega}{2\pi}\left(\frac{3}{2}\chi_M - \chi_K\right) \bmod 1, \tag{6}$$

where Ω is the Frank angle. The disclination structure in Fig. 4(a) has a Frank angle $\Omega = -2\pi/6$. This disclination structure has a fractional charge of $Q_{\mathrm{dis}} = (2/3) \bmod 1$ bound to the disclination core. The bulk-disclination correspondence is manifested in the fractional disclination charge and the localized states bound to the disclination core. The fractional disclination charge can also be understood by counting the number of the Wannier centers. Each unit cell in the disclination region [green in Fig. 4(a)] has four bulk Wannier centers, which gives a 4/3 spectral charge per unit cell. The other two Wannier centers are obstructed by the disclination boundary and thus form localized disclination states. The five unit cells close to the disclination core give in total a fractional spectral charge of 20/3, which is 2/3 modulo 1. We remark that these results are quite different from the 1/4 disclination charge in Ref. [80] and the 1/2 disclination charge in Ref. [76].

To visualize the bulk-disclination correspondence in our PhC, we calculate the eigenstates and the LDOS of photons for the disclination structure in Fig. 4(a). The photonic

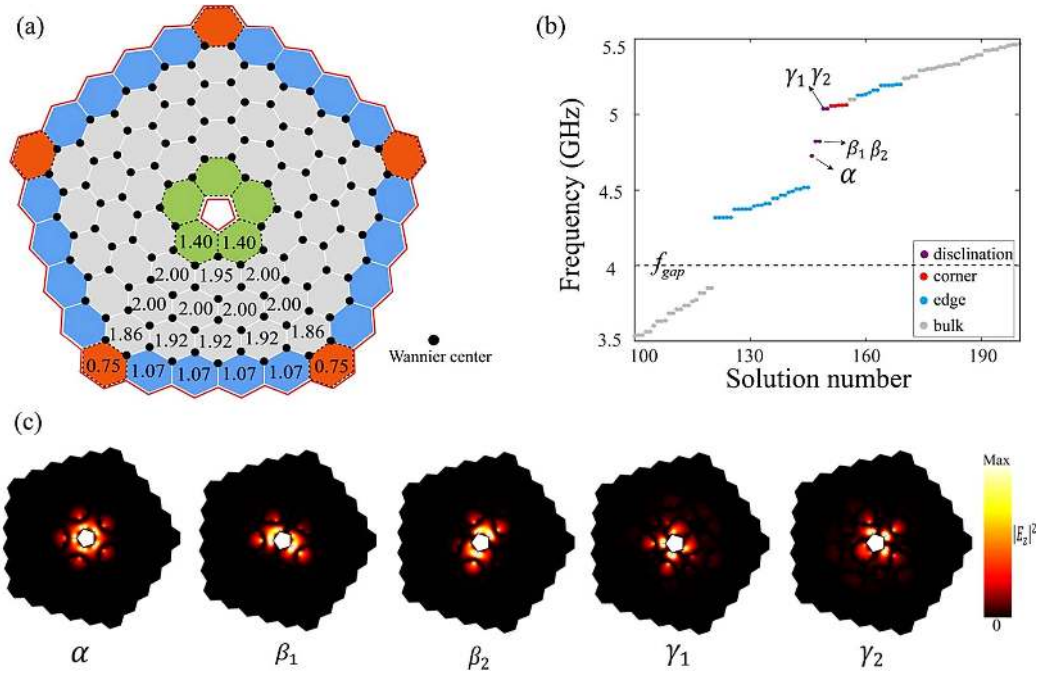

Fig. 4. (a) Spectral charges for various unit cells in a finite disclination structure from the first-principle calculations. Integrating the calculated photonic LDOS up to the frequency $f_{\mathrm{gap}} = 4$ GHz gives the spectral charges presented in the figure. (b) Spectrum of the photonic eigenstates for the finite-sized disclination structure. (c) The five localized states bound to the disclination core. In all calculations, a thin layer of air with the width $0.08a$ is set between the outside PEC boundary and the PhC and another layer of air with the width $0.03a$ is set between the inner PEC boundary and the PhC.

spectrum [Fig. 4(b)] shows that there are five disclination states in the bulk band gap, in addition to the edge states. By integrating the photonic LDOS up to a frequency in the band gap, $f_{\text{gap}} = 4$ GHz, we calculate the spectral charges for all the unit cells. Due to the five-fold rotation symmetry of the disclination structure, we present the spectral charges only for part of the disclination [see Fig. 4(a)]. Again, each bulk unit cell has a spectral charge close to 2, while each edge unit cell has a spectral charge approximately 1. The disclination unit cells have spectral charges of 1.4, which is close to the theoretical value of 4/3.

5. DISCLINATION IN THE TRIVIAL PHOTONIC CRYSTAL

We now study the disclination structure for the trivial PhC. Specifically, we study the PhC with $d/a = 0.25$ and consider the photonic band gap between the first and the second bands. For the band gap, the topological indices are trivial (i.e., $\chi_M = \chi_K = 0$), and the Wannier center of the first band lies at the center of the unit cell [see Fig. 5(a)].

We calculate the spectral charge for each unit cell by integrating the photonic LDOS from zero up to a frequency $f'_{\text{gap}} = 3.2$ GHz in the concerned photonic band gap, as shown in Fig. 5(b). The results in Fig. 5(a) indicate that all the spectral charges are close to 1. There is no signature of charge fractionalization in the disclination structure. Note that the charge has to be fractionalized to integer times of 1/3 or 1/2, not to other fractional values, according to the bulk-disclination correspondence [i.e., Eq. (6)]. Moreover, there is no disclination state. All the eigenstates are bulk states.

6. ROBUSTNESS OF THE DISCLINATION STATES

In this section, we study the robustness of the disclination states against two kinds of disorder: (i) defects that preserve the five-fold rotation symmetry of the disclination (i.e., at the center of the disclination core); and (ii) defects that break such rotation symmetry (i.e., away from the center of the disclination core). The defect is realized by inserting a dielectric rod with a radius of 2 mm but with varying relative permittivity. To facilitate the discussions, we remove the PEC boundary in the disclination core. Such a setup creates a hollow core in the disclination. As a consequence, a defect photonic mode emerges at the disclination core in the trivial PhC. In the meanwhile, there are still five disclination states localized around the disclination core.

We then compare the robustness of the frequencies of the disclination states and the defect state against the same disorder. Specifically, we study the shift of the frequencies of the disclination states and the defect mode as functions of the relative permittivity of the inserted dielectric rod (acting as a defect), which ranges from 1 to 20 in the simulation. To show the robustness of the disclination states, we comparatively study two cases: the disclination structure formed by the photonic TCI with $d/a = 0.46$, and the disclination structure formed by the photonic NI with $d/a = 0.24$. The former has five disclination states, while the latter has a defect mode localized at the hollow disclination core. These two cases are adopted because they have the photonic band gaps with nearly the same band-gap-to-mid-gap ratio of 20%. The position of the defect rod is indicated in the insets in Fig. 6 by the black, blue, and red dots, respectively. We compare the robustness of the frequencies of the disclination states and the defective state in responses to the same disorder. The frequency of the same disclination state (α, β or γ) or defect state changes as a function of relative permittivity of dielectric rod and is summarized in the same figure. The results are presented in Fig. 6 where three different configurations of the disorder are studied for both the TCI and NI. Specifically, Figs. 6(a)–6(c) show, respectively, the effects of the defect pillar on the frequencies of the disclination states in the TCI. Figure 6(d) shows the effects of the defect pillar on the frequencies of the defect state in the NI. It is seen that the frequency shifts of the disclination states in the TCI are much smaller than the frequency shift of the defect state in the NI. Thus, the frequencies of the disclination states in the TCI are more robust than the frequency of the defect state in the NI. These cases correspond to defect configurations that break the five-fold rotation symmetry of the original disclination structure. Thus, the double-degeneracy in the β and γ states is lifted.

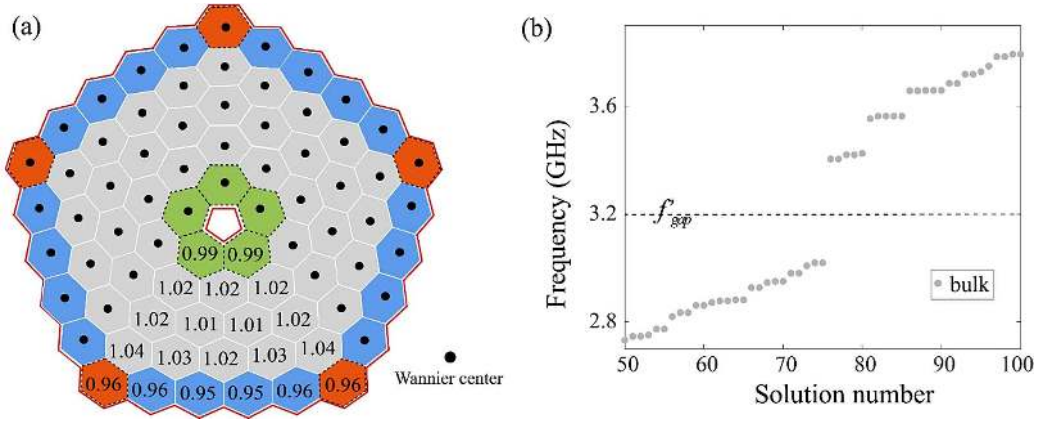

Fig. 5. (a) Wannier center distributions in the disclination structure for the trivial PhC with $d/a = 0.25$. No fractional spectral charge is accumulated since the localized position of Wannier center is at the center of each unit cell. (b) Photonic spectrum of the disclination structure for the trivial PhC. There is no disclination state. Only bulk states are found. In all calculations, a thin layer of air with the width $0.08a$ is set between the outside PEC boundary and the PhC and another layer of air with the width $0.03a$ is set between the inner PEC boundary and the PhC.

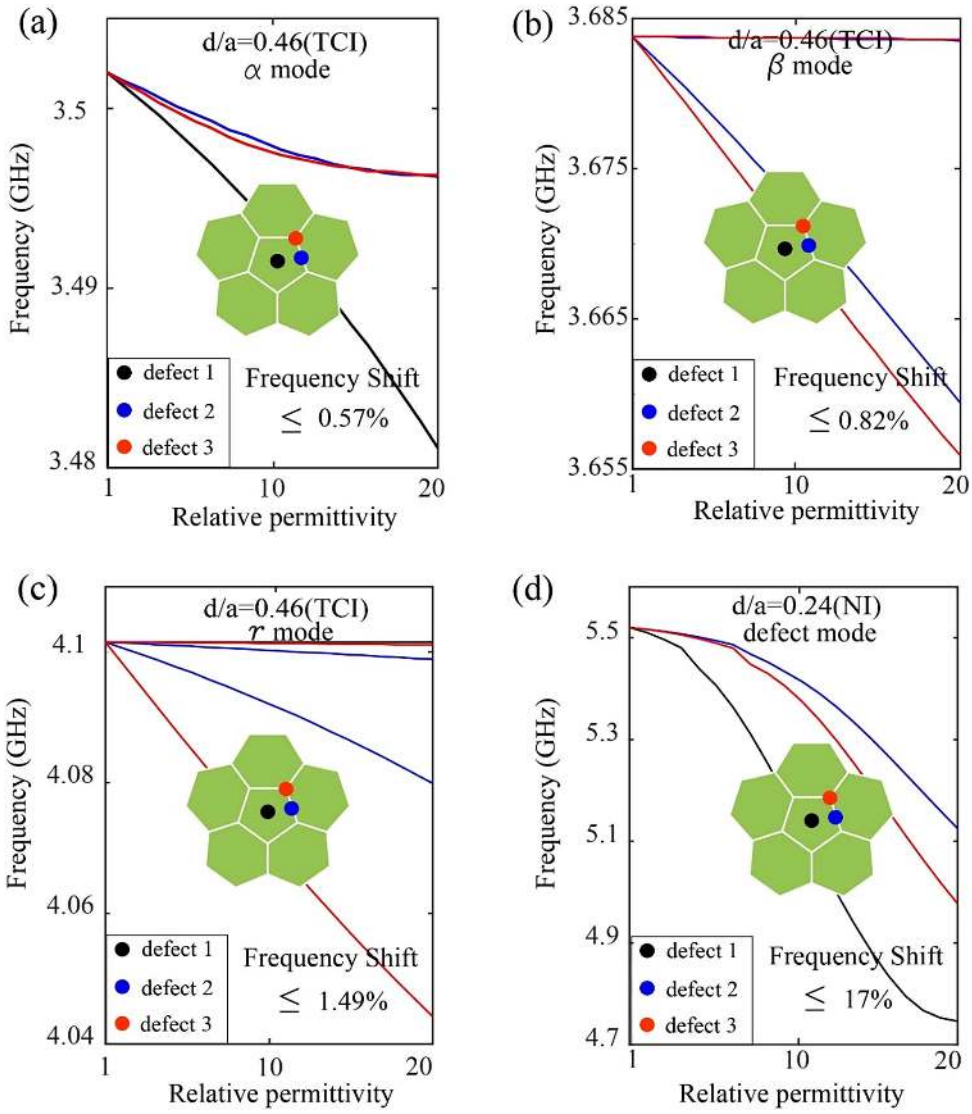

Fig. 6. Frequency shift of the disclination and defect states when the disclination structure contains an additional dielectric rod near the disclination core. The location of the defect rod is indicated by the black, blue, and red dots in the insets. The radius of the defect pillar is 2 mm. We study the frequency shifts of the disclination and defect states as functions of the relative permittivity of defect rod. Frequency of disclination states (α, β, or γ) and defect state as functions of the relative permittivity of the dielectric rod for three different defects is summarized in (a)–(c) and (d), respectively.

Nevertheless, the resilience of the frequencies of the disclination states in the TCI over the frequency of the defective state in the NI remains visible.

7. CONCLUSIONS AND OUTLOOK

We propose a hexagonal PhC with unconventional higher-order topology. In addition to the conventional spectral features of HOTIs (i.e., gapped edge states and in-gap corner states), the unique band topology here gives rise to a fractional charge of 2/3 at the corner boundaries, which is confirmed by the first-principle calculations through the concept of spectral charges. The spectral charges measure the number of photonic modes within a local area (e.g., a unit cell) for all the bulk states below the band gap. We also show that the bulk-disclination correspondence leads to a fractional spectral charge of 1/3 at the disclination core. Besides, we find that there are five localized states bound to the disclination, which is robust against disorders when compared to the conventional defect mode in PhCs. In contrast, the above phenomena disappear in trivial photonic band gaps.

The localized states bound to disclinations can be used as photonic cavity modes that are robust against disorders. Such robust subwavelength cavities are useful in integrated photonic systems as well as for quantum photonics. In addition, these cavity modes can also be exploited for lasing, as demonstrated in recent works. The fractional charges at the corners and disclination cores can be used to control the LDOS of the

bulk photonic states. Our work may inspire future studies on similar phenomena and their applications in photonic and optoelectronic systems.

Funding. Jiangsu Higher Education Institutions (12074281); National Natural Science Foundation of China (12047541).

Acknowledgment. J.-H. Jiang is supported by the Jiangsu specially appointed professor funding, and a project funded by the Priority Academic Program Development of Jiangsu Higher Education Institutions (PAPD).

Disclosures. The authors declare no conflicts of interest.

REFERENCES

1. B. A. Bernevig, T. L. Hughes, and S. C. Zhang, "Quantum spin Hall effect and topological phase transition in HgTe quantum wells," Science **314**, 1757–1761 (2006).
2. L. Fu and C. L. Kane, "Topological insulators with inversion symmetry," Phys. Rev. B **76**, 045302 (2007).
3. M. Z. Hasan and C. L. Kane, "Colloquium: topological insulators," Rev. Mod. Phys. **82**, 3045–3067 (2010).
4. X. L. Qi and S. C. Zhang, "Topological insulators and superconductors," Rev. Mod. Phys. **83**, 1057–1110 (2011).
5. Z. Wang, Y. Chong, J. D. Joannopoulos, and M. Soljačić, "Observation of unidirectional backscattering-immune topological electromagnetic states," Nature **461**, 772–775 (2009).
6. M. Hafezi, E. A. Demler, M. D. Lukin, and J. M. Taylor, "Robust optical delay lines with topological protection," Nat. Phys. **7**, 907–912 (2011).
7. M. C. Rechtsman, J. M. Zeuner, Y. Plotnik, Y. Lumer, D. Podolsky, F. Dreisow, S. Nolte, M. Segev, and A. Szameit, "Photonic Floquet topological insulators," Nature **496**, 196–200 (2013).
8. M. Hafezi, S. Mittal, J. Fan, A. Migdall, and J. M. Taylor, "Imaging topological edge states in silicon photonics," Nat. Photonics **7**, 1001–1005 (2013).
9. A. B. Khanikaev, S. H. Mousavi, W. K. Tse, M. Kargarian, A. H. MacDonald, and G. Shvets, "Photonic topological insulators," Nat. Mater. **12**, 233–239 (2013).
10. W. J. Chen, S. J. Jiang, X. D. Chen, B. Zhu, L. Zhou, J. W. Dong, and C. T. Chan, "Experimental realization of photonic topological insulator in a uniaxial metacrystal waveguide," Nat. Commun. **5**, 5782 (2014).
11. L. H. Wu and X. Hu, "Scheme for achieving a topological photonic crystal by using dielectric material," Phys. Rev. Lett. **114**, 223901 (2015).
12. L. Xu, H. X. Wang, Y. D. Xu, H. Y. Chen, and J. H. Jiang, "Accidental degeneracy in photonic bands and topological phase transitions in two-dimensional core-shell dielectric photonic crystals," Opt. Express **24**, 18059–18071 (2016).
13. X. Cheng, C. Jouvaud, X. Ni, S. H. Mousavi, A. Z. Genack, and A. B. Khanikaev, "Robust reconfigurable electromagnetic pathways within a photonic topological insulator," Nat. Mater. **15**, 542–548 (2016).
14. S. Wu, Y. Wu, and J. Mei, "Topological helical edge states in water waves over a topographical bottom," New J. Phys. **20**, 023051 (2018).
15. Y. Yang, Y. F. Xu, T. Xu, H. X. Wang, J. H. Jiang, X. Hu, and Z. H. Hang, "Visualization of a unidirectional electromagnetic waveguide using topological photonic crystals made of dielectric materials," Phys. Rev. Lett. **120**, 217401 (2018).
16. M. I. Shalaev, W. Walasik, A. Tsukernik, Y. Xu, and N. M. Litchinitser, "Robust topologically protected transport in photonic crystals at telecommunication wavelengths," Nat. Nanotechnol. **14**, 31–34 (2019).
17. X. T. He, E. T. Liang, J. J. Yuan, H. Y. Qiu, X. D. Chen, F. L. Zhao, and J. W. Dong, "A silicon-on-insulator slab for topological valley transport," Nat. Commun. **10**, 872 (2019).
18. S. Barik, A. Karasahin, C. Flower, T. Cai, H. Miyake, W. DeGottardi, M. Hafezi, and E. Waks, "A topological quantum optics interface," Science **359**, 666–668 (2018).
19. S. Mittal, E. A. Goldschmidt, and M. Hafezi, "A topological source of quantum light," Nature **561**, 502–506 (2018).
20. B. Bahari, A. Ndao, F. Vallini, A. E. Amili, Y. Fainman, and B. Kanté, "Nonreciprocal lasing in topological cavities of arbitrary geometries," Science **358**, 636–640 (2017).
21. P. St-Jean, V. Goblot, E. Galopin, A. Lemaitre, T. Ozawa, L. L. Gratiet, I. Sagnes, J. Bloch, and A. Amo, "Lasing in topological edge states of a one-dimensional lattice," Nat. Photonics **11**, 651–656 (2017).
22. G. Harari, M. A. Bandres, Y. Lumer, M. C. Rechtsman, Y. D. Chong, M. Khajavikhan, D. N. Christodoulides, and M. Segev, "Topological insulator laser: theory," Science **359**, eaar4003 (2018).
23. M. A. Bandres, S. Wittek, G. Harari, M. Parto, J. Ren, M. Segev, D. N. Christodoulides, and M. Khajavikhan, "Topological insulator laser: experiments," Science **359**, eaar4005 (2018).
24. Y. Ota, R. Katsumi, K. Watanabe, S. Iwamoto, and Y. Arakawa, "Topological photonic crystal nanocavity laser," Commun. Phys. **1**, 86 (2018).
25. H. Zhao, P. Miao, M. H. Teimourpour, S. Malzard, R. El-Ganainy, H. Schomerus, and L. Feng, "Topological hybrid silicon microlasers," Nat. Commun. **9**, 981 (2018).
26. Y. V. Kartashov and D. V. Skryabin, "Two-dimensional topological polariton laser," Phys. Rev. Lett. **122**, 083902 (2019).
27. Y. Zeng, U. Chattopadhyay, B. Zhu, B. Qiang, J. Li, Y. Jin, L. Li, A. G. Davies, E. H. Linfield, B. Zhang, and Y. Chong, "Electrically pumped topological laser with valley edge modes," Nature **578**, 246–250 (2020).
28. H. Zhong, Y. Li, D. Song, Y. V. Kartashov, Y. Zhang, Y. Zhang, and Z. Chen, "Topological valley Hall edge state lasing," Laser Photon. Rev. **14**, 2000001 (2020).
29. S. Klembt, T. H. Harder, O. A. Egorov, K. Winkler, R. Ge, M. A. Bandres, M. Emmerling, L. Worschech, T. C. H. Liew, M. Segev, C. Schneider, and S. Hofling, "Exciton-polariton topological insulator," Nature **562**, 552–556 (2018).
30. W. Liu, Z. Ji, Y. Wang, G. Modi, M. Hwang, B. Zheng, V. J. Sorger, A. Pan, and R. Agarwal, "Generation of helical topological exciton-polaritons," Science **370**, 600–604 (2020).
31. T. Ozawa, H. M. Price, A. Amo, N. Goldman, M. Hafezi, L. Lu, M. C. Rechtsman, D. Schuster, J. Simon, O. Zilberberg, and I. Carusotto, "Topological photonics," Rev. Mod. Phys. **91**, 015006 (2019).
32. W. A. Benalcazar, B. A. Bernevig, and T. L. Hughes, "Quantized electric multipole insulators," Science **357**, 61–66 (2017).
33. J. Langbehn, Y. Peng, L. Trifunovic, F. von Oppen, and P. W. Brouwer, "Reflection-symmetric second-order topological insulators and superconductors," Phys. Rev. Lett. **119**, 246401 (2017).
34. Z. Song, Z. Fang, and C. Fang, "(d – 2)-dimensional edge states of rotation symmetry protected topological states," Phys. Rev. Lett. **119**, 246402 (2017).
35. W. A. Benalcazar, B. A. Bernevig, and T. L. Hughes, "Electric multipole moments, topological multipole moment pumping, and chiral hinge states in crystalline insulators," Phys. Rev. B **96**, 245115 (2017).
36. F. Schindler, A. M. Cook, M. G. Vergniory, Z. Wang, S. S. P. Parkin, B. A. Bernevig, and T. Neupert, "Higher-order topological insulators," Sci. Adv. **4**, eaat0346 (2018).
37. M. Ezawa, "Higher-order topological insulators and semimetals on the breathing Kagome and pyrochlore lattices," Phys. Rev. Lett. **120**, 026801 (2018).
38. G. van Miert and C. Ortix, "Higher-order topological insulators protected by inversion and rotoinversion symmetries," Phys. Rev. B **98**, 081110 (2018).
39. W. A. Benalcazar, T. Li, and T. L. Hughes, "Quantization of fractional corner charge in C_n-symmetric higher-order topological crystalline insulators," Phys. Rev. B. **99**, 245151 (2019).
40. M. Serra-Garcia, V. Peri, R. Süsstrunk, O. R. Bilal, T. Larsen, L. G. Villanueva, and S. D. Huber, "Observation of a phononic quadrupole topological insulator," Nature **555**, 342–345 (2018).
41. C. W. Peterson, W. A. Benalcazar, T. L. Hughes, and G. Bahl, "A quantized microwave quadrupole insulator with topologically protected corner states," Nature **555**, 346–350 (2018).
42. S. Imhof, C. Berger, F. Bayer, J. Brehm, L. W. Molenkamp, T. Kiessling, F. Schindler, C. H. Lee, M. Greiter, T. Neupert, and

R. Thomale, "Topolectrical-circuit realization of topological corner modes," Nat. Phys. **14**, 925–929 (2018).
43. J. Noh, W. A. Benalcazar, S. Huang, M. J. Collins, K. P. Chen, T. L. Hughes, and M. C. Rechtsman, "Topological protection of photonic mid-gap defect modes," Nat. Photonics **12**, 408–415 (2018).
44. H. Xue, Y. Yang, F. Gao, Y. Chong, and B. Zhang, "Acoustic higher-order topological insulator on a Kagome lattice," Nat. Mater. **18**, 108–112 (2019).
45. X. Zhang, H. X. Wang, Z. K. Lin, Y. Tian, B. Xie, M. H. Lu, Y. F. Chen, and J. H. Jiang, "Second-order topology and multidimensional topological transitions in sonic crystals," Nat. Phys. **15**, 582–588 (2019).
46. H. Fan, B. Xia, L. Tong, S. Zheng, and D. Yu, "Elastic higher-order topological insulator with topologically protected corner states," Phys. Rev. Lett. **122**, 204301 (2019).
47. H. Xue, Y. Yang, G. Liu, F. Gao, Y. Chong, and B. Zhang, "Realization of an acoustic third-order topological insulator," Phys. Rev. Lett. **122**, 244301 (2019).
48. X. Zhang, B. Y. Xie, H. F. Wang, X. Xu, Y. Tian, J. H. Jiang, M. H. Lu, and Y. F. Chen, "Dimensional hierarchy of higher-order topology in three-dimensional sonic crystals," Nat. Commun. **10**, 5331 (2019).
49. M. Weiner, X. Ni, M. Li, A. Alù, and A. B. Khanikaev, "Demonstration of a third-order hierarchy of topological states in a three-dimensional acoustic metamaterial," Sci. Adv. **6**, eaay4166 (2020).
50. Y. Qi, C. Qiu, M. Xiao, H. He, M. Ke, and Z. Liu, "Acoustic realization of quadrupole topological insulators," Phys. Rev. Lett. **124**, 206601 (2020).
51. X. Zhang, Z. K. Lin, H. X. Wang, Z. Xiong, Y. Tian, M. H. Lu, Y. F. Chen, and J. H. Jiang, "Symmetry-protected hierarchy of anomalous multipole topological band gaps in nonsymmorphic metacrystals," Nat. Commun. **11**, 65 (2020).
52. X. Ni, M. Li, M. Weiner, A. Alu, and A. B. Khanikaev, "Demonstration of a quantized acoustic octupole topological insulator," Nat. Commun. **11**, 2108 (2020).
53. H. Xue, Y. Ge, H. X. Sun, Q. Wang, D. Jia, Y. J. Guan, S. Q. Yuan, Y. Chong, and B. Zhang, "Observation of an acoustic octupole topological insulator," Nat. Commun. **11**, 2442 (2020).
54. Y. Wu, M. Yan, H. X. Wang, F. Li, and J. H. Jiang, "On-chip higher-order topological micromechanical metamaterials," arXiv:2010.16242 (2020).
55. Z. K. Lin, H. X. Wang, Z. Xiong, M. H. Lu, and J. H. Jiang, "Anomalous quadrupole topological insulators in two-dimensional nonsymmorphic sonic crystals," Phys. Rev. B. **102**, 035105 (2020).
56. Z. Xiong, Z. K. Lin, H. X. Wang, X. Zhang, M. H. Lu, Y. F. Chen, and J. H. Jiang, "Corner states and topological transitions in two-dimensional higher-order topological sonic crystals with inversion symmetry," Phys. Rev. B **102**, 125144 (2020).
57. F.-F. Li, H.-X. Wang, Z. Xiong, Q. Lou, P. Chen, R.-X. Wu, Y. Poo, J.-H. Jiang, and S. John, "Topological light-trapping on a dislocation," Nat. Commun. **9**, 2462 (2018).
58. X. D. Chen, W. M. Deng, F. L. Shi, F. L. Zhao, M. Chen, and J. W. Dong, "Direct observation of corner states in second-order topological photonic crystal slabs," Phys. Rev. Lett. **122**, 233902 (2019).
59. B. Y. Xie, G. X. Su, H. F. Wang, H. Su, X. P. Shen, P. Zhan, M. H. Lu, Z. L. Wang, and Y. F. Chen, "Visualization of higher-order topological insulating phases in two-dimensional dielectric photonic crystals," Phys. Rev. Lett. **122**, 233903 (2019).
60. S. Mittal, V. V. Orre, G. Zhu, M. A. Gorlach, A. Poddubny, and M. Hafezi, "Photonic quadrupole topological phases," Nat. Photonics **13**, 692–696 (2019).
61. A. El Hassan, F. K. Kunst, A. Moritz, G. Andler, E. J. Bergholtz, and M. Bourennane, "Corner states of light in photonic waveguides," Nat. Photonics. **13**, 697–700 (2019).
62. L. Zhang, Y. Yang, Z. K. Lin, P. Qin, Q. Chen, F. Gao, E. Li, J. H. Jiang, B. Zhang, and H. Chen, "Higher-order topological states in surface-wave photonic crystals," Adv. Sci. **7**, 1902724 (2020).
63. M. Li, D. Zhirihin, M. Gorlach, X. Ni, D. Filonov, A. Slobozhanyuk, A. Alù, and A. B. Khanikaev, "Higher-order topological states in photonic Kagome crystals with long-range interactions," Nat. Photonics **14**, 89–94 (2020).
64. Y. Yang, Z. Jia, Y. Wu, R. C. Xiao, Z. H. Hang, H. Jiang, and X. C. Xie, "Gapped topological kink states and topological corner states in honeycomb lattice," Sci. Bull. **65**, 531–537 (2020).
65. B. Xie, G. Su, H. F. Wang, F. Liu, L. Hu, S. Y. Yu, P. Zhan, M. H. Lu, Z. Wang, and Y. F. Chen, "Higher-order quantum spin Hall effect in a photonic crystal," Nat. Commun. **11**, 3768 (2020).
66. X. Zhou, Z. K. Lin, W. Lu, Y. Lai, B. Hou, and J. H. Jiang, "Twisted quadrupole topological photonic crystals," Laser Photon. Rev. **14**, 2000010 (2020).
67. Y. Chen, Z. K. Lin, H. Chen, and J. H. Jiang, "Plasmon-polaritonic quadrupole topological insulators," Phys. Rev. B **101**, 041109 (2020).
68. L. He, Z. Addison, E. J. Mele, and B. Zhen, "Quadrupole topological photonic crystals," Nat. Commun. **11**, 3119 (2020).
69. Y. Chen, F. Meng, Y. Kivshar, B. Jia, and X. Huang, "Inverse design of higher-order photonic topological insulators," Phys. Rev. Res. **2**, 023115 (2020).
70. W. Zhang, X. Xie, H. Hao, J. Dang, S. Xiao, S. Shi, H. Ni, Z. Niu, C. Wang, K. Jin, X. Zhang, and X. Xu, "Low-threshold topological nanolasers based on the second-order corner state," Light Sci. Appl. **9**, 109 (2020).
71. H. R. Kim, M. S. Hwang, D. Smirnova, K. Y. Jeong, Y. Kivshar, and H. G. Park, "Multipolar lasing modes from topological corner states," Nat. Commun. **11**, 5758 (2020).
72. S. Yves, R. Fleury, T. Berthelot, M. Fink, F. Lemoult, and G. Lerosey, "Crystalline metamaterials for topological properties at subwavelength scales," Nat. Commun. **8**, 16023 (2017).
73. Y. Li, Y. Sun, W. Zhu, Z. Guo, J. Jiang, T. Kariyado, H. Chen, and X. Hu, "Topological LC-circuits based on microstrips and observation of electromagnetic modes with orbital angular momentum," Nat. Commun. **9**, 4598 (2018).
74. M. A. Gorlach, X. Ni, D. A. Smirnova, D. Korobkin, D. Zhirihin, A. P. Slobozhanyuk, P. A. Belov, A. Alù, and A. B. Khanikaev, "Far-field probing of leaky topological states in all dielectric metasurfaces," Nat. Commun. **9**, 909 (2018).
75. N. Parappurath, F. Alpeggiani, L. Kuipers, and E. Verhagen, "Direct observation of topological edge states in silicon photonic crystals: spin, dispersion, and chiral routing," Sci. Adv. **6**, eaaw4137 (2020).
76. Y. Liu, S. Leung, F. F. Li, Z. K. Lin, X. Tao, Y. Poo, and J. H. Jiang, "Bulk–disclination correspondence in topological crystalline insulators," Nature **589**, 381–393 (2021).
77. J. Ahn, D. Kim, Y. Kim, and B. J. Yang, "Band topology and linking structure of nodal line semimetals with Z_2 monopole charges," Phys. Rev. Lett. **121**, 106403 (2018).
78. C. W. Peterson, T. Li, W. A. Benalcazar, T. L. Hughes, and G. Bahl, "A fractional corner anomaly reveals higher-order topology," Science **368**, 1114–1118 (2020).
79. T. Li, P. Zhu, W. A. Benalcazar, and T. L. Hughes, "Fractional disclination charge in two-dimensional C_n-symmetric topological crystalline insulators," Phys. Rev. B **101**, 115115 (2020).
80. C. W. Peterson, T. Li, W. Jiang, T. L. Hughes, and G. Bahl, "Trapped fractional charges at bulk defects in topological insulators," Nature **589**, 376–380 (2021).